REPOLARIZATION CURRENTS IN EMBRYONIC CHICK ATRIAL HEART CELL AGGREGATES

ALVIN SHRIER* AND JOHN R. CLAY‡
*Department of Physiology, McGill University, McIntyre Building, Montreal, Quebec, Canada H3G 1Y6; and ‡Laboratory of Biophysics, IRP, NINCDS, National Institutes of Health at the Marine Biological Laboratory, Woods Hole, Massachusetts 02543

ABSTRACT Outward membrane currents in aggregates of atrial cells prepared from 7–12-d-old chick embryonic hearts were measured with the two microelectrode voltage-clamp technique. Two outward current components, I_{x_1} and I_{x_2}, were found in the plateau potential range of the action potential. The I_{x_1} component is activated between −50 and −20 mV; the I_{x_2} component is activated between −15 and +20 mV. The I_{x_1} component inwardly rectifies, whereas I_{x_2} has an approximately linear current-voltage relation. These preparations lack a time-dependent pacemaker current component, even though they beat spontaneously with an interbeat interval of ~1 s. A mathematical model of electrical activity is described based on our measurements of time-dependent outward current, and measurements in the literature of inward current components.

INTRODUCTION

Within the past few years a number of workers have measured specific ion membrane currents in aggregates of embryonic chick heart cells using the microelectrode voltage clamp technique. The components that have been reported include the excitatory inward sodium current, I_{Na} (Nathan and DeHaan, 1979; Ebihara et al., 1980), the slow inward current I_{si} (Josephson and Sperelakis, 1982), the pacemaker current, I_{K_2} (Clay and Shrier, 1981*a*), and the potassium and sodium ion background currents, I_{K_1} and $I_{Na,b}$ (Clay and Shrier, 1981*a*). The pacemaker and background currents undergo changes during the latter part of embryonic development (Shrier and Clay, 1980; Clay and Shrier, 1981*b*), whereas the other components appear to remain unchanged subsequent to the first week of development (Nathan and DeHaan, 1978; Clay and Shrier, 1981*b*). All of these results were derived from ventricular heart cell aggregates. The electrical activity of embryonic atrial heart cell aggregates is similar to that of ventricular cell preparations, although there are differences in detail. For example, the action potential duration of atrial cells is shorter than that of ventricular cells and the shapes of the pacemaker phases in the two cell types are different (Shrier and Clay, 1982). The latter result is attributable, in part, to a lack of pacemaker current in atrial cells, which we previously reported for 12-d-old preparations. In this paper we extend this analysis of pacemaker mechanisms to 7-d-old atrial cells. We also report two kinetically distinct outward components, I_{x_1} and I_{x_2} in the plateau range of membrane potentials in 7–12-d-old cells, regardless of the stage of development. Both currents appear to be selective to potassium ions. We have incorporated these results in a model of electrical activity that demonstrates spontaneous pacemaker depolarization. The model also illustrates the relationship of outward plateau currents to the repolarization phase of the action potential. An abstract of some of these results has appeared (Shrier et al., 1984).

METHODS

Tissue Culture Preparation

The techniques used to prepare heart cell aggregates were similar to those previously described (Clay and Shrier, 1981*a*). The atria were dissected from hearts of White Leghorn chick embryos incubated at 37°C for 7–12 d. The tissue was dissociated into its component cells in 0.05% trypsin (1:300, Nutritional Biochemical Co.) by the multiple-cycle trypsinization process described elsewhere (DeHaan, 1967, 1970). An inoculum of cells was added to an Erlenmeyer flask containing culture medium 818A (DeHaan, 1970) which consists, by volume, of 25% M199 (Gibco, Grand Island, NY), 2% heat-inactivated, selected horse serum (K. C. Biologicals, Lenexa, KA), 4% heat-inactivated fetal calf serum (Gibco) and 0.5% gentamycin (Schering Corp., Bloomfield, NJ) in a balanced salt solution, which contained (in millimoles per liter): NaCl, 116.0; $MgSO_4$, 0.8; NaH_2PO_4, 0.9; $CaCl_2$, 1.8; $NaHCO_3$, 26.2; glucose, 5.5; KCl, 1.3. The flask was gassed with 5% CO_2, 10% O_2, 85% N_2, sealed with a silicone rubber stopper, and placed on a gyratory shaker (62 rev/min, 1¼-in. stroke) for 48–72 h at 37°C to allow spherical aggregates to form (Sachs and DeHaan, 1973). The contents of each flask were transferred to a plastic tissue culture dish (T = 37°C) on the warm stage of a dissecting microscope. The tissue culture dish was perfused with medium 818P, which was similar to 818A, except that it lacked serum.

Electrophysiological Techniques

Records of spontaneous activity and membrane currents during voltage clamp were obtained using techniques similar to those previously described (Clay and Shrier, 1981*a*). Two glass microelectrodes, each containing 3 M KCl, were impaled within two different cells widely spaced in the aggregate. Electrode resistance was typically 50 MΩ. Standard voltage-clamp circuitry was used. Electrical activity and membrane currents in response to rectangular voltage clamp steps were recorded on a Hewlett-Packard (3964A) tape recorder at 3¾ in/s (DC-1250 Hz) for off-line analysis. Perfusate containing 1 μM tetrodo-

toxin (TTX) was used in all voltage clamp measurements to suppress excitability and the underlying fast, inward sodium current, I_{Na}.

The suitability of heart cell aggregates for voltage clamp analysis has been demonstrated elsewhere. The cells within an aggregate are well-coupled electrically, during spontaneous activity and in voltage clamp conditions (DeHaan and Fozzard, 1975; DeFelice and DeHaan, 1977; Nathan and DeHaan, 1979; Mathias et al., 1981). The input capacitance is directly proportional to D^3, where D is the aggregate diameter, and the input resistance at any given membrane potential is proportional to D^{-3} (Clay et al., 1979). These results indicate that membrane potential changes occur uniformly throughout the aggregate (Clay et al., 1979). Moreover, our measurements of potassium current kinetics in the vicinity of the potassium equilibrium potential are adequately described by single exponential functions of time, which is consistent with our treatment of a heart-cell aggregate as a lumped circuit with minimal ion accumulation or depletion in the extracellular spaces of the preparation (Clay and Shrier, 1981*a*).

Data Analysis

Membrane currents were filtered (low-pass; 3 db cutoff at 200 Hz) and digitized. These results were fitted by a mathematical program based on the Rissanen (1978) criterion, which determines from least-squares minimization the optimal fit with the fewest number of exponential components. The general outcome of this analysis was that the currents generated in response to positive-directed steps from holding potentials in the -40 to -10 mV range were optimally described by a single exponential function of time (I_{x_2}). The tail currents following return to holding level were also optimally fit by single exponentials. The current in response to a negative going step was also fitted with a single exponential (I_{x_1}). The reactivation current following return to the holding level consisted of a rapid component, which was attributed to I_{si}, and a slow component (I_{x_1}). Some records, such as the -51 and -61 mV records in Fig. 4, exhibited a small, slow drift. These results required a second exponential term with a time constant of several seconds. The addition of this term in the analysis changed the best fit value of the time constant of the more rapid exponential component by no more than 20%.

Computer Simulation Technique

Our simulations were based on the equation relating membrane potential, V, to membrane current, $I(V)$,

$$dV/dt = -I(V)/C_i, \quad (1)$$

where $I(V)$ is the sum of the ionic currents in Table I and C_i is the input capacitance. We used C_i = 0.0063 μf in our simulations, which is appropriate for an aggregate having a diameter of 130 μm, the size of our model preparation (Clay et al., 1979). The I_{x_1}, I_{x_2}, I_{Na}, and I_{si} components are time-dependent, gated currents (Table I) that are described by the general relationship $dy/dt = -y/\tau_y + \alpha_y$, where y represents the gating parameter, τ_y represents the time constant of the gating parameter, and α_y represents the forward rate constant from the closed to open states of the gating parameter. For example, y corresponds to x_1 for the I_{x_1} current, and τ_y and α_y correspond to the τ_{x_1} and α_{x_1}, respectively. We implemented our simulations with an Euler iteration technique (Moore and Ramon, 1974) for Eq. 1 and a Rush and Larsen (1978) iteration technique for the gating parameters. The iteration time step was varied throughout the course of any given simulation in order to achieve a compromise between computational speed and accuracy.

RESULTS

Spontaneous Activity

Aggregates of 7–12-d-old chick atrial cells usually beat spontaneously with an interbeat interval typically in the 0.5 to 2.0 s range. We have observed spontaneous beating lasting several days from aggregates maintained in suspension in flasks placed on a gyratory shaker. Moreover, we have recorded, by optical methods, regular, spontaneous beating from aggregates in culture dishes over a period of several hours, at which time these experiments were terminated. These results demonstrate that our tissue culture conditions, in particular our K_o = 1.3 mM culture conditions, are sufficient to maintain the ionic concentration gradients across the cellular membranes of these preparations. A representative recording of the membrane potential changes associated with spontaneous activity is shown in Fig. 1. The maximum rate of rise of the upstroke phase of the action potential in this preparation was 120 V/s, the maximum overshoot potential was 25 mV, the maximum diastolic potential (MDP) was -85 mV, and the action potential duration (APD) measured between the times of occurrence of the maximum overshoot and maximum diastolic potentials was 82 ms. During the pacemaker phase, the membrane potential spontaneously depolarized from MDP to approximately -75 mV within the first 100 ms following the time of occurrence of MDP. It subsequently depolarized to threshold in a very gradual manner. Addition of tetrodotoxin to the culture medium at a concentration of 1 μM blocked the activity in these preparations resulting in a resting potential typically in the -75 to -50 mV range.

Current-Voltage Relation

The current-voltage relations for an aggregate of 12-d-old atrial cells in three different levels of external potassium ion concentration (K_o = 1.3, 3, and 5 mM) are shown in Fig. 2. These results correspond to the total, net membrane current at the end of 5 s duration voltage clamp steps from a holding potential of -26 mV. Similar results were obtained with a more traditional holding level of -60 mV. The net current in the pacemaker range of membrane potentials (-90 to -65 mV) was relatively small for all three levels of K_o. It appeared to be insensitive to K_o in

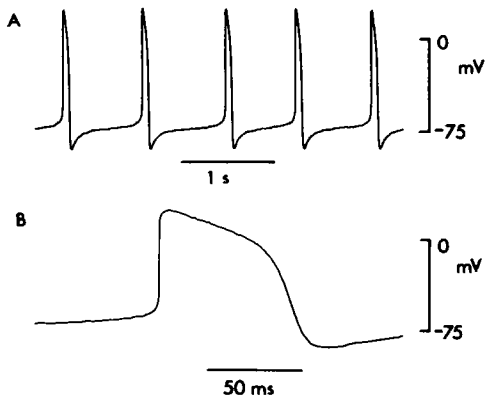

FIGURE 1 Spontaneous activity from an aggregate of 12-d-old atrial cells. Aggregate diameter D was 150 μm.

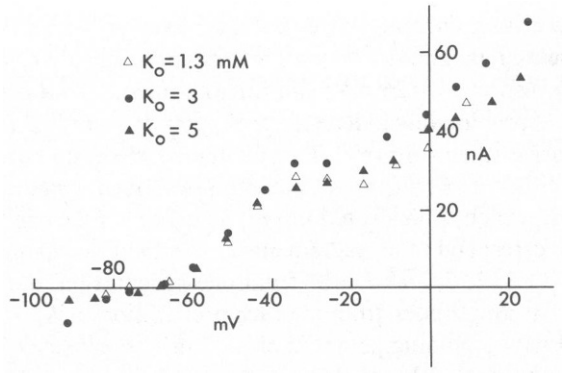

FIGURE 2 Current-voltage relations from an aggregate of 12-d-old atrial cells in three different potassium ion concentrations. D = 130 μm. Membrane currents were measured at the end of 5 s voltage-clamp steps. Holding potential was −26 mV.

contrast to our previously published results of pacemaker current from ventricular cell aggregates (Clay and Shrier, 1981*a*). The net current for potentials positive to −65 mV increased monotonically with membrane potential in the −65 to −35 mV range; it was approximately independent of potential for $-35 \leq V \leq -15$ mV, and it monotonically increased with membrane potential for V > 15 mV. The net current for $V > -40$ mV was sensitive to changes in K_o, particularly when K_o was increased from 1.3 to 3 mM, as illustrated in Fig. 2. However, the current-voltage relation did not exhibit the "cross-over" effect with increases in K_o, in contrast to results from ventricular cells (Clay and Shrier, 1981*a*). Results similar to those in Fig. 2 were obtained from a total of eight aggregates regardless of the stage of development within the 7–12-d incubation period.

Pacemaker Current

We did not observe a time-dependent current of either the I_f (DiFrancesco, 1981) or I_{K_2} type (Clay and Shrier, 1981*a*) in the pacemaker potential range (−95 to −65 mV) in these experiments. This result is illustrated in Fig. 3 for an aggregate of 7-d-old atrial cells. The membrane potential was held at −66 mV in this experiment. Voltage steps to −83 and −93 mV revealed a small time-independent, or background, current and a lack of a significant time-dependent component, which is in marked contrast to our original observations from 7-d-old ventricular aggregates under similar experimental conditions (Shrier and Clay, 1980). The implications of this result for the spontaneous pacemaker process are discussed below. In some experiments large hyperpolarizing steps to potentials negative to the pacemaker voltage range revealed a hint of a time-dependent component, which we have not analyzed in this study.

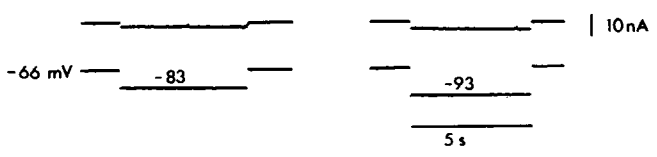

FIGURE 3 Lack of time-dependent pacemaker current from an aggregate of 7-d-old atrial cells. D = 150 μm. K_o = 1.3 mM.

Voltage Clamp Protocol for Measurements of Repolarization Currents

We observed two kinetically distinct, time-dependent, outward currents for voltage clamp pulses positive to $V = -60$ mV. One component was activated in the −50 to −20 mV potential range; the other component was activated at potentials positive to $V = -15$ mV. We have termed these currents I_{x_1} and I_{x_2} to be consistent with the notation of McAllister et al. (1975). We measured current kinetics with a holding potential typically within a few mV of −20 mV, although holding potentials throughout the −60 to −10 mV range were also used. The steady current level at −20 mV was approximately 20 nA (Fig. 2). In some experiments the membrane potential was held at similarly depolarized levels for as long as 30 min, which involved the passage of a considerable amount of potassium ions into the cell impaled by the current passing electrode. However, the cells in the aggregate are well coupled electrically, as noted above (Methods). Therefore, the passage of potassium ions into the aggregate is balanced by the passage of ions from the aggregate to the external medium (volume ~1 cc). The resulting change in the external potassium ion concentration was estimated to be <1 μM. Holding the preparation at depolarized levels for long durations did not have any apparent deleterious effect. The holding current changed by no more than 10% throughout these experiments, and the current kinetics measured at the beginning of each experiment were consistent with measurements at the end of each experiment. The rationale for using depolarized holding levels was twofold. One reason is that V approximately equal to −20 mV was intermediate to the ranges of activation of the I_{x_1} and I_{x_2} components. Consequently, a hyperpolarizing pulse relative to the holding potential revealed time-dependent current due primarily to I_{x_1}, and a depolarizing pulse revealed time-dependent current due primarily to I_{x_2}. The second rationale for depolarized holding levels is that the calcium current component, I_{si}, is substantially inactivated under these conditions, as noted by Josephson and Sperelakis (1982) based on measurements from preparations similar to ours. For example, they observed a lack of inward current at the end of 300 ms voltage steps for membrane depolarizations that elicited a significant inward current transient. They also observed a lack of an effect of verapamil (10^{-6} M) on the steady-state current at depolarized potentials. These results demonstrate that embryonic chick heart cells do not have a significant noninactivating I_{si} component. Our records in Fig. 18 are also consistent with this result, as noted below.

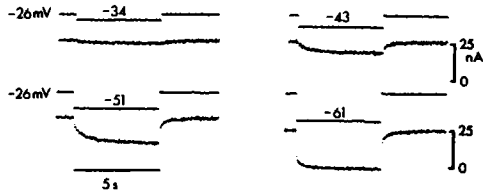

FIGURE 4 Voltage clamp measurements of I_{x_1}. Same preparation as in Fig. 2. K_o = 1.3 mM.

I_{x_1} Kinetics

Representative records of the I_{x_1} component are illustrated in Fig. 4. The holding potential, V_H, was −26 mV in this experiment; the step potentials illustrated in Fig. 4 are −34, −43, −51, and −61 mV. The time-dependent currents during these steps are attributable to deactivation of the I_{x_1} component. The amplitude of time-dependent current as a function of step potential increased as the step potential was made increasingly negative (Fig. 4) with a maximum amplitude occurring at approximately −70 mV with K_o = 1.3 mM. Below −70 mV the current amplitude diminished as the step potential approached E_K, the potassium equilibrium potential. Qualitatively similar results were obtained for all holding potentials in the −40 to −10 mV range. These results indicate inward rectification of the I_{x_1} channel with negative slope conductance positive to V = −70 mV.

The time-dependent currents upon return to the holding level describe reactivation of I_{x_1}. Consequently, the latter results define the voltage range of activation of I_{x_1}. This

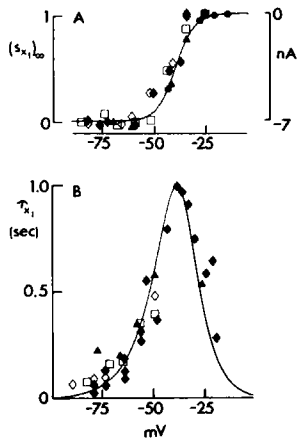

FIGURE 5(*A*) Voltage dependence of I_{x_1} activation. The right hand scale corresponds to the amplitude of reactivation current upon return to holding potential (−26 mV), as described in the text. The solid curve is a description of these results by $(s_{x_1})\infty = \alpha_{x1}/(\alpha_{x1} + \beta_{x1})$, as described by Eqs. 2 and 3 in the text. The symbols represent K_o = 1.3 (♦); K_o = 3 mM (◇); K_o = 5 mM (□); and K_o = 7 mM (▲). All of these results were taken from a single preparation. The results represented by (●) were taken from a second aggregate in K_o = 1.3 mM with a holding potential of −62 mV. These results were shifted 10 mV in the hyperpolarizing direction as described in the text. (*B*) Time constants of I_{x_1}. The solid curve represents $\tau_{x_1} = (\alpha_{x1} + \beta_{x1})^{-1}$, as described in the text. The symbols represent the same K_o conditions, as given above. Pooled results from three aggregates.

reactivation current was essentially zero for −34 mV; it increased in amplitude with increasingly negative steps with respect to −26 mV; and it had a maximal value that was approximately independent of potential for steps more negative than −50 mV. That is, the reactivation current amplitude as a function of potential described a sigmoidal curve, which is illustrated in Fig. 5 *A*. The symbols in Fig. 5 *A* correspond to measurements of reactivation current in K_o = 1.3, 3, 5, and 7 mM from one preparation and tail current amplitudes from another preparation in K_o = 1.3 mM with a holding potential of −62 mV (see below). The scale to the right of Fig. 5 *A* represents the absolute measurements for K_o = 3 and 7 mM and V_H = −26 mV. The maximal reactivation current in these conditions was −7 nA, relative to the holding current. The maximal reactivation current for K_o = 1.3 and 5 mM was −6.2 and −6.7 nA, respectively. The results in Fig. 5 *A* for these two levels of K_o were scaled by 7/6.2 and 7/6.7, respectively. All data points were then scaled by 7 nA to give the normalized activation curve of the I_{x_1} component (left hand scale of Fig. 5 *A*). The solid line in Fig. 5 *A* is the best fit to these results of $(s_{x_1})_\infty = \alpha_{x_1}/(\alpha_{x_1} + \beta_{x_1})$ where

$$\alpha_{x_1} = \alpha_0 \exp [\alpha_1(V - V_1)] \quad (2)$$

and

$$\beta_{x_1} = \beta_0 \exp [\beta_1 (V - V_1)], \quad (3)$$

with best fit parameters α_0 = 23 s^{-1}, α_1 = 0.12 mV^{-1}, β_0 = 0.036 s^{-1}, β_1 = −0.09 mV^{-1}, and V_1 = −14 mV. The solid line in Fig. 5 *B* is the best fit to the I_{x_1} time constants, τ_{x_1}, by $(\alpha_{x_1} + \beta_{x_1})^{-1}$ with α_{x_1} and β_{x_1} given by Eqs. 2 and 3, respectively, with the parameters given above, except for V_1, which was −17 rather than −14 mV.

The measurements of reactivation current in Fig. 4 suggest that I_{x_1} is fully activated for V approximately equal

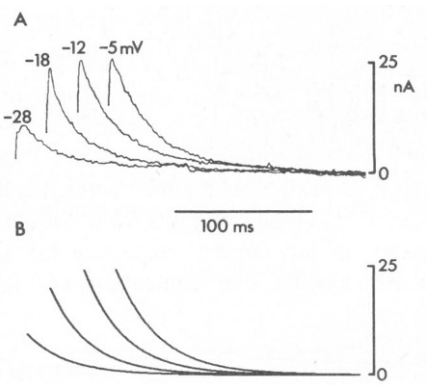

FIGURE 6 I_{x_1} tail currents. (*A*) The membrane potential was held for 10 s at the indicated potentials before being stepped to −62 mV in each case. The membrane current 5 ms after each step is shown here. The initial, rapidly rising phase of each record is due to capacitative current. (*B*) Best fits to the records in *A* by single exponential functions of time with a time constant of 35.6, 34, 35.1, and 36 ms for the −28, −18, −12, and −5 mV records, respectively.

to −20 mV. We further tested this point in another preparation with tail current measurements at a potential of −62 mV (Fig. 6 *A*). In this experiment the membrane potential was held for 10 s at −28, −18, −12, or −5 mV followed by a step to −62 mV. The resulting tail currents were adequately described by single exponential functions of time, as illustrated in Fig. 6 *B*. The time constants of the best fit exponentials were 35.6, 34, 35.1, and 36 ms for the −28, −18, −12, and −5 mV records, respectively. The initial tail current amplitudes at $V = -12$ and −5 mV were the same, demonstrating that I_{x_1} is fully activated for V less than −12 mV. The relative amplitudes of these currents are plotted in Fig. 5 *A*. The I_{x_1} activation curve of the preparation from which the −62 mV records were obtained was approximately 10 mV positive with respect to the I_{x_1} reactivation curve for the preparation from which the −26 mV holding potential results were obtained. Consequently, the −62 mV results were shifted 10 mV in the hyperpolarizing direction to enhance the comparison with the reactivation currents from the experiment described in Fig. 4.

Measurements of I_{x_1} were carried out in a total of six aggregates. The position on the voltage axis at which the current was 50% activated was −30 ±5 mV (±SD). The maximum I_{x_1} time constant was 0.95 ±0.15 s. The amplitude of the fully activated current was 22.2 ±9.6 nA.

I_{x_1} Reversal Potential

The I_{x_1} component is a potassium selective current, as illustrated in Fig. 7. In this experiment the membrane potential was held at −26 mV, as in Fig. 4, and it was stepped in 10 mV increments to successively more negative levels until current reversal occurred. We then changed the command potential by 1 mV steps in order to find the potential level, E_K, for which essentially no time-dependent current resulted. The results for E_K for the preparation in Fig. 7 were −103 mV, −91 mV, and −82 mV for $K_o = 3$ (not shown), 5, and 7 mM, respectively. The value of E_K was determined several times in this experiment for each level of K_o using various different intervals between clamp steps ranging between 3 and 15 s. No dependence of E_K on the time between steps was observed. The range of variation of the measurements of E_K for each level of K_o was ~1 mV. Similar measurements of E_K were obtained from four other preparations with $K_o = 1.3$ mM and two other preparations with $K_o = 4.3$ mM. The value of E_K with $K_o = 1.3$ mM was −113 ±4.3 mV (±SD). The values of E_K for the two preparations with 4.3 mM K_o were −87 and −92 mV, respectively.

The shift in E_K with K_o described above and in Fig. 7 is consistent with the equivalent result for a potassium electrode with $K_i = 145$ mM. The results in Fig. 7 also illustrate our fitting procedure. The time-dependent currents in Fig. 7 are superimposed upon single exponential curves which are essentially indistinguishable from the data.

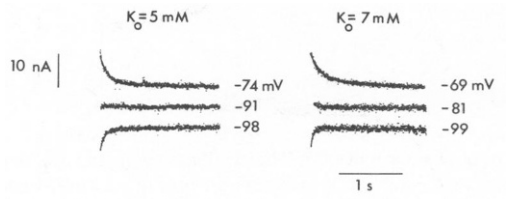

FIGURE 7 Reversal potential for I_{x_1}. Each record is the membrane current response for steps to the potentials indicated. Each record is superimposed upon a solid curve that is the best fit to these results of a single exponential function. Holding potential was −26 mV.

I_{x_1} Current-Voltage Relation

We determined the instantaneous, fully-activated current-voltage relation for the I_{x_1} channel from the ratio of the amplitude of the time-dependent current following a voltage step and the time-dependent current upon return to the holding level (Noble and Tsien, 1968; Clay and Shrier, 1981*a*). The results of this analysis are illustrated in Fig. 8 for $K_o = 1.3$, 3, 5, and 7 mM. The I_{x_1} current-voltage (*I-V*) relation inwardly rectified and it had negative slope conductance for potentials more than 30 mV positive to E_K. The negative slope character of the I_{x_1} *I-V* is apparent from the records in Fig. 4 as noted above. For example, the voltage step to $V = -51$ mV elicited a time-dependent response that had a greater amplitude than that of the reactivation current upon return to holding potential. Consequently, the ratio of time-dependent current was >1 for this step. The ratio was reduced as the step voltage approached E_K, and it was negative for potentials less than

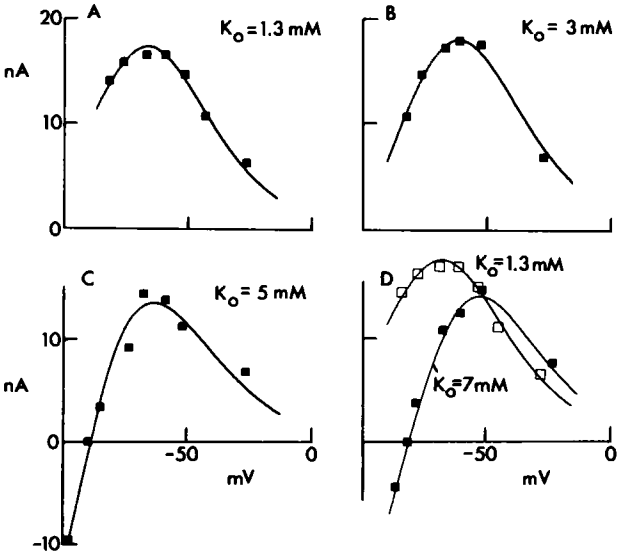

FIGURE 8 Current-voltage relations for I_{x_1}, as determined from ratio analysis of records such as those in Fig. 4. The solid curves are theoretical representations of these results of Eq. 4 in the text. The parameters $I^0_{x_1}$ and G_1 in Eq. 4 are as follows: $K_o = 1.3$ mM; $I^0_{x_1} = 0.69$ μA, $G_1 = 0.018$; K_o = mM; $I^0_{x_1} = 0.68$ μA, $G_1 = 0.058$; $K_o = 5$ mM; $I^0_{x_1} = 0.54$ μA, $G_1 = 0.49$; $K_o = 7$ mM; $I^0_{x_1} = 0.47$ μA, $G_1 = 0.23$.

E_K because the time-dependent current reversed direction, as illustrated in Fig. 7. The absolute amplitude of the *I-V* was determined by multiplying these ratio results by the maximum reactivation current amplitude. The results of this analysis are illustrated in Fig. 8. The shape of the *I-V* curve was approximately independent of K_o (Fig. 8). The primary effect of a change in K_o was to shift the *I-V* relation along the voltage axis by an amount equal to the corresponding shift of E_K. This point is illustrated in Fig. 8 *D*, which contains the current-voltage relations for K_o = 1.3 mM (Fig. 8 *A*) and K_o = 7 mM. The maximal outward current in K_o = 7 mM was ~25% less than it was in K_o = 1.3 mM. Moreover, the current-voltage relations crossed over at $V = -50$ mV, which is an effect that appears to be common to most types of potassium channels in muscle membranes that display inward-directed rectification. These results are similar to the effects of K_o on the fully activated I_{K_2} component (Clay and Shrier, 1981*a*).

The curves in Fig. 8 are best fits to the data of a model of single-file diffusion of potassium ions through a membrane channel. The model contains a blocking particle that is kept out of the channel by inward current, and is knocked into the channel by outward movement of ions, thereby producing inward rectification (Clay and Shrier, 1981*a*; Clay and Shlesinger, 1984). The model is described by

$$I_{x_1}(V) = I^0_{x_1}(p_+ - (K_o/K_i)p_-)y^2(1 - G_1)G_1^{-1}/(1 + y + y^2(1 - G_1)G_1^{-1}), \quad (4)$$

where $I^0_{x_1}$ and G_1 are constants that are given in the legend of Fig. 8, and K_i and K_o are the internal and external potassium ion concentrations, respectively, and $p_+ = [1 + \exp(-V/25)]^{-1}$, $p_- = 1 - p_+$, and $y = K_o p_-/(K_i p_+)$. The various parameters in Eq. 4 are described in Clay and Shlesinger (1984). Ions move through the channel in this model only when collisions of permeant ions from either the internal or external solution strike the channel with sufficient energy to overcome the forces that tend to keep ions in place in the channel. When such a collision occurs, the probability that outward movement occurs is p_+, and the probability that inward movement occurs is p_-. The probability that the blocking particle moves into the channel during outward movement is G_1.

I_{x_2} Kinetics

The results in Fig. 9 are representative records of the I_{x_2} component which was activated by voltage steps positive to $V = -15$ mV. The net current jumped instantaneously in the negative direction immediately after the voltage steps in the records in Fig. 9 because of the negative slope character of I_{x_1}, which was fully activated at the holding level. A slight inflection, or sigmoidicity, is apparent during the initial 100 ms of these records. The sigmoidicity was independent of holding potential (−45 to −10 mV). We fitted the I_{x_2} results by single exponential functions of time, as illustrated in Fig. 10 for the steps in Fig. 9 with

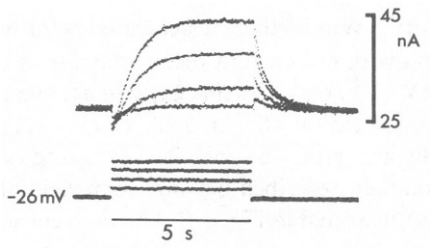

FIGURE 9 Superimposed voltage clamp measurements of I_{x_2} for $V = -17, -9, -1, 8$ mV. Same preparation as in Fig. 2 and Fig. 4. K_o = 1.3 mM.

$V = -1$ and 8 mV. A slightly better fit to our I_{x_2} results during the initial 100 ms of these records could be obtained with a model (not shown) consisting of two closed states and one open state. (A single exponential raised to a power did not fit these results.) We opted for the simpler analysis, because a single exponential did provide an adequate description of these results, as can be ascertained by comparing the data points with the solid lines in Fig. 10. The normalized tail current and the time constants for I_{x_2} are shown in Fig. 11, *A* and *B*, respectively. The theoretical curves in Fig. 11 are best fits to these results of $s_{x_2} = \alpha_{x2}/(\alpha_{x_2} + \beta_{x_2})$ and $\tau_{x2} = (\alpha_{x_2} + \beta_{x_2})^{-1}$, respectively, where

$$\alpha_{x_2} = \alpha^0_{x_2}(V + V_2)/\{1 - \exp[\alpha^1_{x_2}(V + V_2)]\} \quad (5)$$

and

$$\beta_{x_2} = \beta^0_{x_2} \exp[\beta^1_{x_2}(V + V_2)] \quad (6)$$

with best fit parameters $\alpha^0_{x_2} = 0.1\ s^{-1}$, $\alpha^1_{x_2} = -0.08\ mV^{-1}$, $\beta^0_{x_2} = 0.195\ s^{-1}$, $\beta^1_{x_2} = -0.055\ mV^{-1}$, and $V_2 = -15$ mV.

Measurements of I_{x_2} were carried out in six aggregates. The position on the voltage axis at which the current was 50% activated was 1 ±5 mV (±SD). The maximum time constant was 0.9 ±0.1 s. The maximum I_{x_2} tail current amplitude was 19.5 ±5.5 nA (n = 5).

I_{x_2} Current-Voltage Relation

The I_{x_2} current-voltage relation, as determined by ratio analysis, is shown in Fig. 11 *C* for K_o = 1.3, 3, and 5 mM.

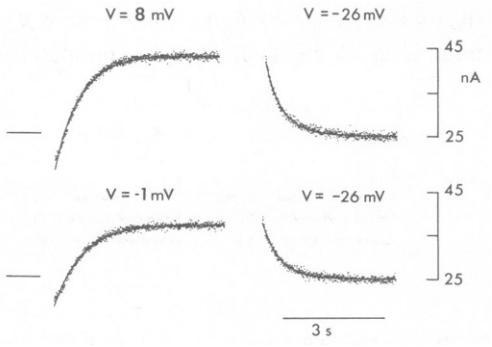

FIGURE 10 Description of I_{x_2} kinetics by single exponential functions of time. Same records as in Fig. 9.

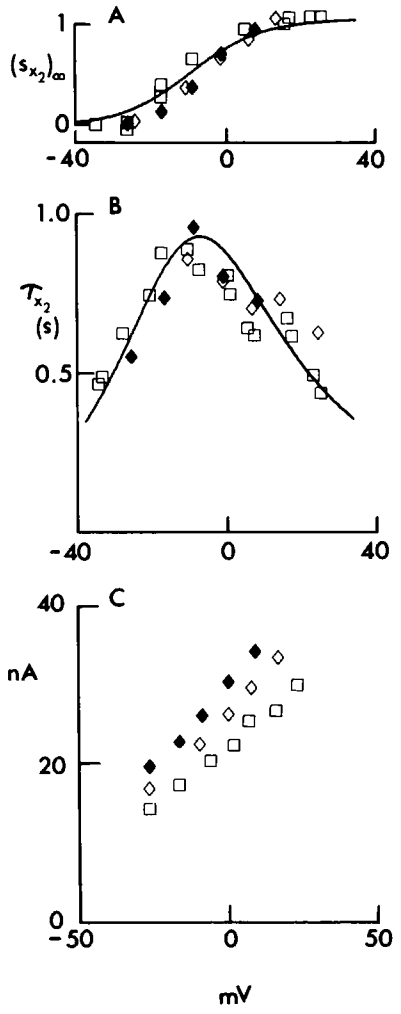

FIGURE 11 (*A*) Normalized tail current amplitudes. The solid curve is a description of these results by $(s_{x_2})_\infty = \alpha_{x_2}/(\alpha_{x_2} + \beta_{x_2})$ as described by Eqs. 5 and 6. (*B*) Time constants of I_{x_2}. The solid curve represents $\tau_{x2} = (\alpha_{x_2} + \beta_{x_2})^{-1}$. (*C*) Current-voltage relations for I_{x_2} as determined from ratio analysis. The symbols in *A*, *B*, and *C* represents K_o = 1.3 mM (♦), K_o = 3 mM (◇), and K_o = 5 mM (□).

These results were approximately described by a linear relation for $-25 \leq V \leq 25$. We did not directly determine the I_{x_2} reversal potential, although the extrapolated reversal potentials from the results in Fig. 11 *C* indicate that I_{x_2} is carried at least partly by potassium ions.

Relative Contributions of I_{x_1} and I_{x_2} to Outward Current

The I_{x_1} and I_{x_2} components are further amplified by the results in Fig. 12, which describe the membrane current response to a voltage step to +8 mV from either −41 (Fig. 12 *A*) or −28 mV (Fig. 12 *B*). The result in Fig. 12 *A* exhibits a small, rapid, outward current (denoted by the arrow), and a slower component (I_{x_2}). We attributed the rapid component in Fig. 12 *A to* I_{x_1}, although this result, by itself, is inadequate to determine the kinetic and ionic

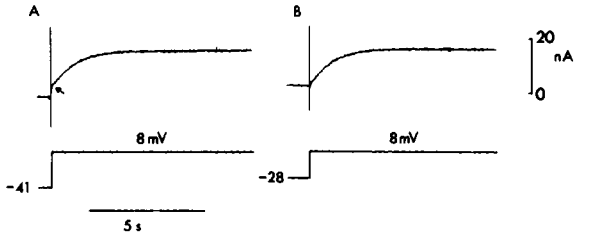

FIGURE 12 Time-dependent current following a voltage step to +8 mV. (*A*) Holding potential, −41 mV. (*B*) Holding potential, −28 mV. The arrow in *A* indicates the contribution of I_{x_1}, although this record, by itself, is inadequate to determine the kinetic and ionic properties of the underlying current. The dominant component in both records is attributable to I_{x_2}. These results are from a different preparation than the one described in Fig. 9.

characteristics of the underlying current. The early component is not apparent in Fig. 12 *B*, because, the I_{x_1} kinetics are almost fully activated at −28 mV in steady-state conditions. These results illustrate the difficulty in measuring I_{x_1} from a holding potential that lies below the I_{x_1} activation curve. The maximum, fully activated I_{x_1} current occurs at $V < -50$ mV (Fig. 8), but $(s_{x_1})_\infty$ at this potential is approximately zero (Fig. 5 *A*). Consequently, the I_{x_1} kinetics are most readily observed with hyperpolarizing steps from a depolarized holding potential, as in Fig. 4. The results in Fig. 12 also demonstrate that the I_{x_2} channel does not inactivate, at least not for steps lasting 9 s, or less. These results, as well as the records in Fig. 9, also provide compelling evidence for a lack of ion-accumulation effects in heart cell aggregates. If ion accumulation were a factor, the membrane current in these records would exhibit a declining phase due to a reduction in driving force, as is apparent in squid axon potassium current records, for example, during long-lasting membrane depolarizations (Frankenhauser and Hodgkin, 1956; Clay, 1984). The I_{x_2} tail kinetics in Figs. 9 and 10 also argue against significant accumulation/depletion effects. These results were consistent with single exponential functions of time (Fig. 10) which is to be expected in the absence of ion accumulation (Hume and Giles, 1983).

Reconstruction of Electrical Activity

We have incorporated our measurements of outward membrane currents with the measurements of I_{Na} by Ebihara et al. (1980) and I_{si} by Josephson and Sperelakis (1982) in a model of electrical activity in atrial heart cell aggregates. The various current components are described in the Appendix and in Table I. The relative contributions of $I_{bg}(I_{K_1} + I_{Na,b})$, I_{x_1} and I_{x_2} to the net, steady-state current of the model are illustrated in Fig. 13. Curve *c* in Fig. 13 represents the I_{bg} component; curve *b* represents $I_{bg} + I_{x_1}(t \rightarrow \infty)$, and curve *a* represents $I_{bg} + I_{x_1}(t \rightarrow \infty)$ and $I_{x_2}(t \rightarrow \infty)$. Most of the current for $V < -30$ mV is attributable to I_{bg}, which is apparent, experimentally, from the −61 mV record in Fig. 4 following return back to the

TABLE I
MEMBRANE CURRENT COMPONENTS

Inward excitatory currents		Kinetic variables
$I_{Na} = \bar{g}_{Na} m^3 hh'(V - E_{Na})$	$\bar{g}_{Na} = 140\ \mu S$ $E_{Na} = 40$ mV	$\alpha_m = -320\,(V + 47.13)/(\exp[-0.1\,(V + 47.13)] - 1)\,s^{-1}$ $\beta_m = 80\exp(-V/11)\ s^{-1}$ $\alpha_h = 135\exp[-(V + 80)/6.8]\ s^{-1}$ $\beta_h = 3{,}560\exp(0.079V) + 3.1 \times 10^8\exp(0.35\,(V + 4))\ s^{-1}$ for $V \leq -40$ $\beta_h = 0$; $\tau_h = 0.13\{\exp[-(V + 10.66)/11.1] + 1\}$ sec for $V > -40$ $\alpha_{h'} = 0.5\exp[-(V + 20)/20]$ $\beta_{h'}\ 0.5\exp[(V + 10)/5]$
$I_{si} = \bar{g}_{si}\, dff'(V - E_{Ca})$	$\bar{g}_{si} = 8.7\ \mu S$ $f_{Ca} = 30$ mV	$\alpha_d = 2600\exp[-0.02(V - 5)]/\{\exp[-0.15\,(V - 5)] + 1\}\,s^{-1}$ $\beta_d = 1780\exp[-0.17(V + 34)]/\{\exp[-0.072\,(V + 34)] + 1\}\,s^{-1}$ $\alpha_f = 0.025\exp(-0.1\,V)\ s^{-1}$ $\beta_f = 0.25\,V/[1 - \exp(-V/5)]\ s^{-1}$ $\alpha_{f'} = 0.5\ s^{-1}$ $\alpha_{Ca} = 130\ nA^{-1}\,s^{-1}$ $\beta_{f'} = 50/\{1 + \exp[0.1(V + 50)]\}\ s^{-1}$ $\beta_{Ca} = 0.0125\ s^{-1}$
Outward time-dependent currents		Kinetic variables
$I_{x_1} = I^0_{x_1} s_{x_1} f_{x_1}(V)$	$f_x(V) = \dfrac{y_1^2(1 - G_2)G_2^{-1}(p_+ - (K_o/K_i)p_-)}{1 + y_1 + y_1^2(1 - G_2)/G_2}$ $G_2 = 0.0186$ $I^0_{x_1} = 870$ nA $y_1 = (K_o p_-)/(K_i p_+)$; $p_+ = [1 + \exp(eV/kT)]^{-1}$; $p_- = 1 - p_+$	$\alpha_{x_1} = 23\exp(0.13(V + 14))s^{-1}$ $\beta_{x_1} = 0.036\exp[-0.09(V + 14)]$
$I_{x_2} = s_{x_2} f_{x_2}(V)$	$f_{x_2}(V) = \dfrac{P_{x_2} F\, eV/kT(K_o - K_i\exp(eV/kT))}{1 - \exp(eV/kT)}$ $P_{x_2} = 0.201 \times 10^{-5}$ cm · s^{-1}	$\alpha_{x_2} = 0.1(V - 15)/\{1 - \exp[-0.08(V - 15)]\}$ $\beta_{x_2} = 0.195\exp[-0.055(V - 15)]$
Background currents		
$I_{K_1} = I^0_{K_1} f^0_{K_1}(V) + I^1_{K_1} f^1_{K_1}(V)$	$f^0_{K_1}(V) = \dfrac{y_0^3(1 - G_0)G_0^{-1}[p_+ - (K^0_o/K_i)p_-]}{1 + y_0 + y_0^2 + y_0^3(1 - G_0)/G_0}$ $f^1_{K_1}(V) = \dfrac{\lvert V + V_R\rvert y_1^2(1 - G_1)G_1^{-1}(p_+ - (K^1_o/K_i)p_-)}{V_R(1 + y_1 + y_1^2(1 - G_1)/G_1)}$ $y_0 = (K^0_o p_-)/(K_i p_+)$; $y_1 = (K^1_o p_-)/(K_i p_+)$ $K^0_o = 1.5$ mM; $K^1_o = 10.7$ mM; $I^0_{K_1} = 14.5\ \mu A$ $I^1_{K_1} = 0.56$ nA; $V_R = 65$ mV; $G_0 = 0.4$; $G_1 = 0.1$	
$I_{Na,b} = \bar{g}_{Na,b}(V - E_{Na})$	$E_{Na} = 40$ mV $\bar{g}_{Na,b} = 0.035\ \mu S$	

holding level (−26 mV). The prediction of the model concerning spontaneous activity is illustrated in Fig. 14 *B* along with the voltage waveform from Fig. 1 *A*, which is reproduced in Fig. 14 *A* to facilitate comparison between experiment and theory. The action potential of the model is shown on an expanded scale in Fig. 14 *C* superimposed on the action potential record from Fig. 1 *B*. The membrane potential at the beginning of the simulation in Fig. 14 *B* was −90 mV and all gating parameters were set equal to zero. The membrane subsequently deplarized to threshold of I_{Na} in ~0.55 s. The rate of pacemaker depolarization following the first and all subsequent action potentials was slowed by a small residual component of I_{x_1}. This pacemaker mechanism is further discussed below. The experimental waveform in Fig. 14 *A* shows some variability in interbeat interval, which could be attributable to membrane noise (Clay and DeHaan, 1979). We did not attempt to simulate this variability. The model is in generally good agreement with the experimental waveform concerning the overall shape of both the action potential and pacemaker phase, as illustrated in Fig. 14 *C*. The voltage and time axes of the model were scaled by 0.94 and 0.86, respectively, to enhance comparison between experiment and the model in Fig. 14 *C*. That is, the amplitude of the model action potential was 121 mV and its duration was 96 ms, as compared with the experimental values of 114 mV and 82 ms, respectively, for the waveform in Fig. 14 *C*. These differences between experiment and theory are not significant. We have observed a range of action potential amplitude of 100 to 130 mV, and a range in APD of 70 to 120

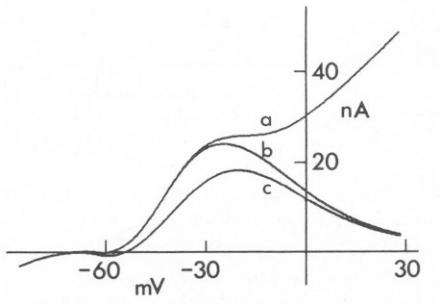

FIGURE 13 Contributions of I_{bg} (I_{K_1} + $I_{Na,b}$), I_{x_1}, and I_{x_2} to the steady-state ionic current in the computer model. Curve *a* represents I_{bg} + I_{x_1} + I_{x_2}; Curve *b* represents I_{bg} + I_{x_1}; Curve *c* represents I_{bg}.

ms. The model parameters are consistent with these experimental results. Both the latter phase of pacemaking and most of the upstroke phase of the action potential overlap with the experimental result almost exactly, following the scaling procedure, as does the initial phase of pacemaking following MDP. The shape of the plateau phase of the action potential differs from experiment. This phase of the waveform was variable. The experimental record in Fig. 14 *C* shows an almost linear region of gradual repolarization during the plateau, which was atypical. For example, compare the record in Fig. 14 *C* with the action potential in Fig. 18 *A*, which has a more rounded appearance. The model also has a rounded appearance, but it does generally fail to describe the initial rate of repolarization during the plateau, which is greater in the experimental waveforms than in the model. This discrepancy between experiment and theory is probably attributable to deficiencies in our model of I_{si}.

The contributions of I_{Na}, I_{si}, I_{x_1}, and I_{x_2} to the activity in Fig. 14 *B* are shown in Fig. 15. The I_{Na} component contributes to the final 50 ms of pacemaking, as illustrated in the panel immediately below the action potential in Fig. 15. This result is similar to the original model of pacemaker activity in cardiac Purkinje fibers by McAllister et al. (1975). The I_{Na} component is rapidly activated during the upstroke of the action potential, which is not shown in Fig. 15, and it is zero during the repolarization phase. The latter effect is attributable to the slow inactivation process, h', as described in the Appendix. However, this parameter is completely inconsequential to repolarization in these simulations. The predictions of the model overlap to within a line width regardless of whether or not the h' parameter is included. This additional inactivation of I_{Na} is important only for conditions that produce rapid firing of the model, which we have not included in this study. The I_{si} component contributes to the latter part of the upstroke phase, and it is approximately constant throughout the plateau of the action potential. It increases slightly during the initial part of repolarization because of the overlap between activation and the inactivation of I_{si} in the platueau range. Further consideration of I_{si} inactivation is given below. The I_{x_1} and I_{x_2} components are activated during the plateau, but

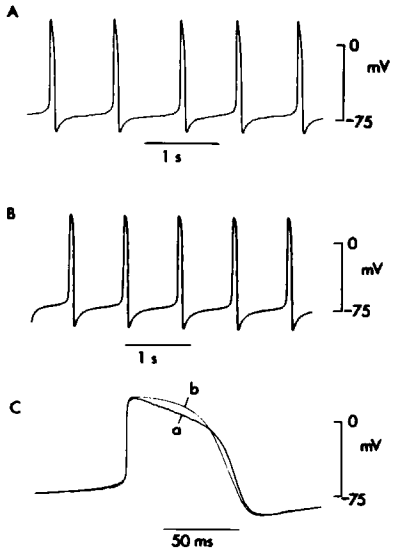

FIGURE 14 (*A*) Experimental recording of spontaneous activity. (*B*) Spontaneous activity predicted by the model. The initial conditions of the simulation were $V = -90$ mV and all gating parameters set equal to zero. Pacemaker depolarization subsequent to the first and all other action potentials is slower than the initial pacemaker event because s_{x_1} is not completely deactivated during repolarization. Consequently, a small component of I_{x_1} contributes to the pacemaker process. (*C*) Comparison of the model (Curve *b*) and experimental (Curve *a*) action potentials. The voltage and time axes of the model were scaled by 0.94 and 0.82, respectively.

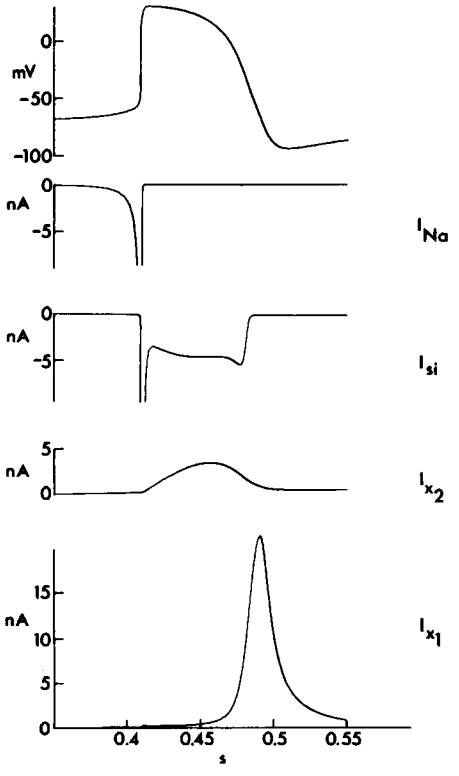

FIGURE 15 Relationship between excitability and the underlying ionic currents, as described in the text.

very little current flows through the I_{x_1} channels because of inward rectification. Moreover, I_{x_2} is only partially activated because the membrane potential does not remain in the platueau long enough for full activation of I_{x_2} to occur. However, I_{x_2} does contribute to the total current during plateau phase, along with I_{si} and $I_{bg}(I_{K_1} + I_{Na,b})$. All three components play a role in controlling action potential duration, as described below. The I_{x_1} component is fully activated during repolarization. Moreover, a small fraction of I_{x_1} channels remain open during the initial 200 ms pacemaker depolarization, which reduces the net inward effect of I_{bg}. This point is further demonstrated by Fig. 16, which illustrates the current-voltage trajectory in the pacemaker potential range (solid line with arrows denoting the direction of voltage change with time) and the steady-state current-voltage relation (dashed line). The difference between the solid and dashed curves in Fig. 15 for $V < -70$ mV is due to I_{x_1}. The trajectory approaches the steady-state relation in the latter part of pacemaking as I_{x_1} deactivates. The trajectory crosses the steady-state relation at V approximately equal to -70 mV due to the initial phase of activation of I_{Na}.

As Fig. 16 demonstrates, the steady-state current-voltage relation in our model lies just slightly below the voltage axis throughout the pacemaker voltage range. Automaticity is, therefore, very sensitive to small changes in I_{bg}. For example, a slight decrease in $\bar{g}_{Na,b}$ which is sufficient to shift the steady-state current-voltage relation slightly above the voltage axis near $V = -70$ mV causes the model to be quiescent. This sensitivity of spontaneous activity to model parameters is reflected in our experimental observations of variability in beat rates within any given sample of atrial preparations, as well as the sensitivity of the beat rate of any single preparation to sustained stimulus currents of relatively small amplitude (Shrier and Clay, 1982).

The respective roles of I_{x_1}, I_{x_2}, and I_{bg} in repolarization are further illustrated by the simulations in Fig. 17. The simulation in Fig. 17 *A* is the same as in Figs. 14 and 15. The I_{x_2} component was removed in Fig. 17 *B*, I_{x_1} was

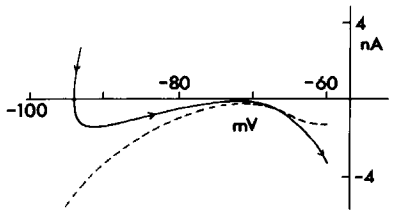

FIGURE 16 Relationship between the current-voltage trajectory during spontaneous activity (solid line with arrows denoting the direction of time) and the steady-state current-voltage relation (dashed line). The trajectory represents the net ionic current during the latter part of repolarization and the pacemaker phase. The deviation between the two curves for $V < -70$ mV is due to I_{x_1}. The s_{x_1} component is zero in the steady-state for $V < -70$ mV, whereas it is slightly greater than zero during pacemaking. The deviation between the two curves for $V > -70$ mV is due to activation of I_{Na}.

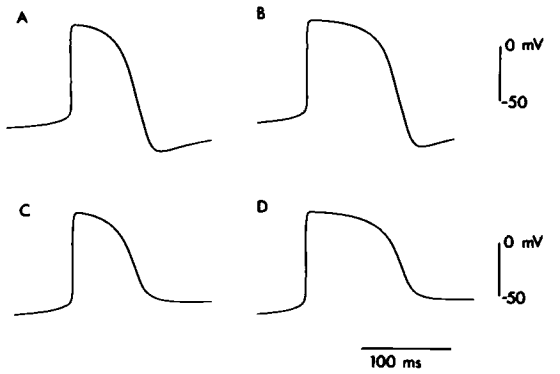

FIGURE 17 Relative contributions of I_{bg}, I_{x_1}, and I_{x_2} to repolarization in the computer model. (*A*) Control model result. Same as in Fig. 14 *C*. (*B*) Model action potential with I_{x_2} eliminated. (*C*) Model action potential with I_{x_1} eliminated. (*D*) Model action potential with both I_{x_1} and I_{x_2} eliminated. The only net outward current in this case was $I_{bg} = I_{K_1} + I_{Na,b}$. The initial potential in all three simulations was -75 mV.

removed in Fig. 17 *C*, and I_{x_1} and I_{x_2} were both removed in Fig. 17 *D*. The result in Fig. 17 *B* demonstrates that I_{x_2} is not a critical factor in determining the overall shape of the action potential, although it is a factor in determining the duration of the plateau. The result in Fig. 17 *D* illustrates the role of I_{bg} $(I_{K_1} + I_{Na,b})$ in repolarization. This component is a key factor in the model, since I_{bg} alone can hyperpolarize the membrane from the maximum overshoot potential to -55 mV with a shape of this phase of the action potential which is qualitatively consistent with experiment.

The contribution of outward current to repolarization is further illustrated experimentally, in Fig. 18. Fig. 18 *A* consists of an action potential from a different preparation than the one described in Fig. 1 superimposed upon the result obtained by holding this preparation in voltage clamp for several seconds at -22 mV, and then releasing the clamp. After a slight initial delay, the membrane potential repolarized from -22 mV with a time course which overlaps almost exactly with the repolarization phase of the action potential. This result demonstrates that these preparations do not contain a significant, noninactivating I_{si} component, as demonstrated directly by Josephson and Sperelakis (1982). If I_{si} were not substantially inactivated at -22 mV, the membrane potential would depolarize toward E_{Ca}, rather than hyperpolarize. An inward current does appear to underlie the initial delay in repolarization, which we have modeled in Fig. 18 *B* by assuming that a slight reactivation of I_{si} occurred immediately following release of the clamp at -22 mV. Fig. 18 *A* also demonstrates that repolarization to potentials more negative than -22 mV is attributable solely to membrane current activated in the steady-state at this potential, i.e., I_{bg} and I_{x_1}, but not I_{x_2}. The role of outward current is further illustrated in Fig. 18 *C* and the corresponding simulations in Fig. 18 *D*. In this experiment the membrane potential was held for several seconds in voltage clamp at -23, -33,

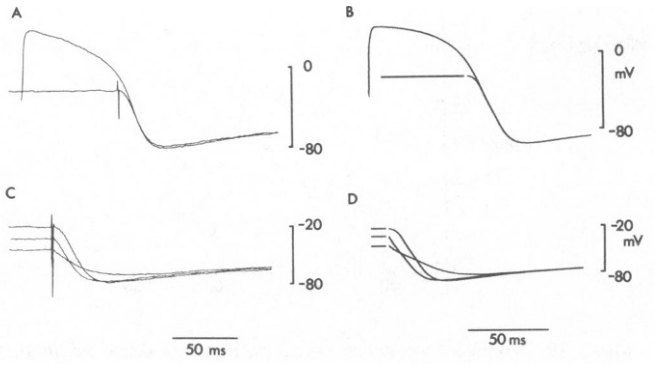

FIGURE 18 (*A*) Superimposed records of an action potential and the record obtained from the same preparation by holding the membrane potential in voltage clamp for several seconds at −22 mV and then releasing the clamp. The time at which the clamp was turned off is indicated by the stimulus artifact. (*B*) Simulations of the results in *A*. The simulated action potential was the same as in Fig. 14 *C*. The simulation following the dashed line was obtained with all gating parameters set at their steady-state values appropriate to $V = -22$ mV. The I_{si} inactivation parameters, f', was initially set at 0.08. (*C*) Superimposed results of three records obtained by holding the preparation in voltage clamp for several seconds at −23, −33, and −45 mV and then releasing the clamp. (*D*) Simulations of the results in *C*. These results were obtained with all parameters of the model set at their steady-state values appropriate to −23, −33, and −45 mV, respectively. The f' parameter was set at 0.08 in each case.

and −45 mV, and the clamp was then released. In all three cases the potential hyperpolarized below the zero current potential of the current-voltage relation (−60 mV) followed by depolarization to threshold of I_{Na}. These results demonstrate, unequivocally, that time-dependent, outward current is activated in the steady-state in the −45 to −20 mV range. The undershoot of membrane potential below −60 mV (Fig. 18 *C*) requires the presence of a time-dependent, inductive element, which we have attributed to I_{x_1}, based on the voltage clamp results in this study.

DISCUSSION

This report is a continuation of our investigation concerning membrane-current components having relatively slow kinetics in embryonic chick heart cell aggregates. We previously reported a time-dependent pacemaker current, I_{K_2}, which was present in 7-d-old ventricular cells, but virtually absent from 17-d-old cells (Shrier and Clay, 1980; Clay and Shrier, 1981*a*, *b*). We did not observe time-dependent pacemaker current of either the I_{K_2} or I_f type (DiFrancesco, 1981) in 7–12-d-old atrial cells, even though these preparations generally beat spontaneously with an interbeat interval typically in the 0.5 to 2 s range. These preparations also lack significant time-independent current in the pacemaker voltage range that effectively results in a very high membrane slope resistance (~200 KΩ·cm^2) near threshold. This feature is of critical significance for producing relatively long interbeat intervals, as described below.

We have observed two kinetically distinct time-dependent currents, I_{x_1} and I_{x_2}, in the plateau range of membrane potentials that contribute to the repolarization phase of the action potential. The current-voltage relation for I_{x_1} inwardly rectifies with negative slope conductance for $V \geq -70$ mV. This result is qualitatively similar to our earlier observations of I_{K_2}, although the voltage range over which the rectification of I_{x_1} occurs is considerably broader than that of I_{K_2}. The other repolarization component, I_{x_2}, is qualitatively similar to I_K in nerve axon (Hodgkin and Huxley, 1952) in its steady-state activation curve and its current-voltage relation. The primary difference is that the I_{x_2} kinetics at 37°C are on the order of hundreds of milliseconds compared with several milliseconds for I_K in nerve at 10°C.

Our measurements are reminiscent of the original report of two repolarization currents in sheep Purkinje fibers by Noble and Tsien (1969), which has been criticized, recently, by Jaeger and Gibbons (1985*a*). Specifically, Jaeger and Gibbons (1985*a*) suggest that cardiac Purkinje fibers do not possess time-dependent, outward plateau currents. They attribute the original observations of Noble and Tsien (1969) to I_{si}, and they suggest that repolarization of the action potential could be due solely to background current (Jaeger and Gibbons, 1985*b*). Recently, Gintant et al (1985) have contributed to this issue based on measurements from isolated canine cardiac Purkinje myocytes. They observed a time-dependent, outward plateau current activated between −40 and −20 mV (similar to the range of activation of our I_{x_1} results), but they did not observe a component that was activated at more positive potentials (I_{x_2}). Their results appear to provide clear cut evidence for the presence of a current in cardiac Purkinje fibers with at least some properties that are similar to the original Noble and Tsien (1969) analysis. Nevertheless, it is important to consider the objections raised by Jaeger and Gibbons (1985*a*). One of the key points of the I_{x_1} analysis is the relationship between the tail current time constant, τ_{tail}, at the holding potential (−60 mV, for example) and the amplitude of a depolarizing step, V_{step}, particularly for depolarizing steps that activate I_{si}. The I_{x_1} analysis requires that τ_{tail} be independent of V_{step}. Jaeger and Gibbons (1985*a*) presented results on this issue (Table III of their paper) that are extremely variable, even for a single preparation, and they argued that the original Noble and Tsien (1969) tail current results were similarly equivocal. Our results in Fig. 6 clearly demonstrate a lack of dependence of τ_{tail} on V_{step}. Specifically, τ_{tail}, obtained from our automated analysis of digitized versions of the records in Fig. 6 *A*, was 35.6, 34, 35.1, and 36 ms for V_{step} equal to −28, −18, −12, and −5 mV, respectively, with a holding level of −61 mV. The tight clustering of these results around a single value (35.3 ms) is consistent with the I_{x_1} analysis. Moreover, the ionic nature of the current activated in the −40 to −20 mV range can be determined, unequivocally, in our preparations by stepping to potentials in the vicinity of E_K. The results in Fig. 7 clearly demon-

strate that this current is carried by potassium ions. Moreover, the results in Fig. 18 *A* and 18 *C* demonstrate that this current does play a key role in repolarization. We agree with Jaeger and Gibbons (1985*b*) that the background current can also play a significant role in this process, as demonstrated by the simulations in Fig. 17 *C*. However, I_{bg} cannot repolarize the membrane to potentials more negative than the zero-current potential of the *I-V* relation (approximately equal to −60 mV). A time-dependent component, I_{x_1}, is required for this part of the action potential.

We believe our I_{x_1} results are not significantly contaminated by I_{si}, as we have argued above, primarily because I_{si} is substantially inactivated at depolarized holding potentials (Josephson and Sperelakis, 1982). It is also important to consider the possibility that our I_{x_2} results may also be contaminated by other voltage- and time-dependent currents. For example, Giles and van Ginnekin (1985) have recently reported a transient outward current (I_A) in rabbit atrial heart cells, which is activated at potentials positive to −20 mV, as is I_{x_2}. However, we believe it is unlikely that an I_A component is contained in our I_{x_2} results, because I_A is also substantially inactivated at positive holding potentials. Moreover, the I_A activation time course for $V \geq -20$ mV is ~10 ms at $T = 20$°C, or ~2 ms at $T = 37$°C based on a Q_{10} of 3. We were not able to resolve current kinetics on this time scale in these experiments.

We have based our analysis on a two-current model of time-dependent plateau current, although we cannot unequivocally rule out the possibility that our results may be described by a single component having complex kinetic and rectification properties. Such a model would have to provide a description of our results that is equivalent to the I_{x_1} and I_{x_2} analysis. Consequently, the mechanism of repolarization that we are proposing would be unchanged. We believe the single component model is unlikely based primarily on the voltage dependence of tail current amplitudes, i.e., saturation of I_{x_1} tails for $V < 0$ mV (Fig. 6) and saturation of I_{x_2} tails for $V > 0$ mV (Fig. 11). To further illustrate this point we have plotted the tail currents from the experiment described by Figs. 5 and 11 on a single axis in Fig. 19. These results demonstrate a staircase voltage dependence of tail current amplitude, which is strongly suggestive of two kinetically distinct current components.

Time-dependent plateau currents have been reported in several cardiac preparations including cat ventricular fibers (McDonald and Trautwein, 1978), frog trabeculae (Ojeda and Rougier, 1974; Brown et al., 1976), and single atrial and ventricular cells from bull frogs (Hume and Giles, 1983; Shibata and Giles, 1985). In particular, Ojeda and Rougier (1974) reported the presence in some of their preparations of two repolarization currents having steady-state activation curves comparable to our results. Several authors have suggested that voltage clamp measurements from atrial trabeculae are complicated by ion accumulation or depletion in the intercellular clefts of these preparations (Noble, 1976; Brown et al., 1980). Our results argue against this effect in small heart cell aggregates, such as the ones we have used, having diameters in the 100–200 μm range. In particular, the close agreement between the I_{x_1} kinetics near E_K with single exponential functions of time and a similar agreement between single exponentials and I_{x_2} kinetics, particularly the I_{x_2} tail kinetics (Hume and Giles, 1983), provides further support for our treatment of aggregates as lumped, space-clamped preparations in which accumulation or depletion of ions in the intercellular spaces is not significant.

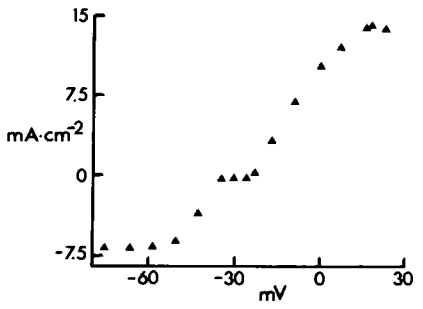

FIGURE 19 Voltage dependence of tail currents, as described in the text.

Our mechanism of pacemaking is consistent with the original results on frog atrial trabeculae of Brown et al. (1976). The time-independent background current is sufficient to depolarize the membrane to threshold of I_{Na} in a slow time-dependent manner, as illustrated by the first pacemaker phase in the simulation in Fig. 13 *B*. The I_{x_1} component was initially set equal to zero in this part of the simulation, and it remained zero throughout the depolarization preceding the initial action potential, because the pacemaker voltage range ($-90 \leq V \leq -65$ mV) lies below the I_{x_1} activation range. The duration of this pacemaker phase was 0.55 s. The duration of all subsequent pacemaker phases in the simulation was 0.75 s. The increase in duration was attributable to I_{x_1}, which continues to flow for approximately 0.2 s following the maximum diastolic potential of the action potential, thereby reducing the rate of diastolic depolarization. The I_{Na} component contributes to depolarization during the final 50 ms of the pacemaker phase, as indicated by the results in Fig. 15. The only current that flows during the intervening 0.5 s is the background current, which must be very small in amplitude to produce the slow rate of depolarization in this phase of the cycle. Consequently, automaticity in these preparations can be disrupted by relatively small current amplitudes either from external sources, or from intrinsic membrane noise. It is tempting, therefore, to speculate that one role of time-dependent current, be it I_f or I_{K_2}, in a primary pacemaker cell may be to maintain rhythmicity in the presence of small fluctuations in membrane current. Indeed, our simulations differ most significantly from similar work on the primary pacemaker (s-a node) with

regard to the pacemaker current component (I_{K_2}, I_f, or I_h). Yanagihara, et al. (1980), Bristow and Clark (1982), Noble and Noble (1984), and Brown et al. (1984) have all carried out simulations in which a current of this type activated in the −90 to −60 mV range was included. The decay of potassium current activated at plateau potentials may also be an important pacing element in these preparations, as Noble (1984) has recently suggested.

APPENDIX

The various current components used in our computer simulations are listed in Table I. The model for the I_{Na} component was taken from Ebihara and Johnson (1980) with a minor modification in the β_h parameter to account for our measurements of the steady-state I_{Na} window current (Atwell et al., 1979) in the −60 to −40 mV membrane potential range (A. Shrier and J. R. Clay, unpublished). We also added an additional inactivation parameter, h', based on the observations of Ebihara et al. (1983). The effect of this modification of the Ebihara and Johnson (1980) model is to eliminate any contribution of the I_{Na} channel to the net membrane current during the repolarization phase of the action potential. That is, h' is set to zero during the plateau and the time constant of its reactivation in the −60 to −40 mV range is approximately 500 ms. It is reset to 1 in the −100 to −90 mV range with a time constant of approximately 25 ms. This parameter is not critical in these simulations, as noted in the Results. Our model of I_{si} is similar to that of Beeler and Reuter (1977) with appropriate modifications in the activation and inactivation parameters, d and f, respectively, to describe the I_{si} kinetic measurements of Josephson and Sperelakis (1982). The measurements of Josephson and Sperelakis (1982) demonstrate a lack of steady-state I_{si} current for all potentials, including the −40 to −10 mV potential range for which d_∞ and f_∞ are both non-zero. We modeled this aspect of I_{si} by a slow inactivation process, f', based on the results of Fischmeister and Horackova (1983), Kass and Sanguinetti (1984), and Lee et al. (1985) which demonstrate that inactivation of calcium channels in heart cells is mediated by Ca entry. The equation describing f' is

$$df'/dt = \beta_{f'} - (\beta_{f'} + ([Ca_i]/[Ca_{i,o}])\alpha'_f)f', \qquad (A1)$$

where $\beta_{f'}$ and α_f are voltage-dependent parameters given in Table I, $[Ca_{i,o}]$ is the resting, internal calcium ion concentration, which we have assumed to be 10^{-7} M, and $[Ca_i]$ is governed by (Beeler and Reuter, 1977)

$$d[Ca_i]/dt = -\alpha_{Ca} I_{si} [Ca_i] + \beta_{Ca}([Ca_{i,o}] - [Ca_i]), \quad (A2)$$

where α_{Ca} and β_{Ca} are also given in Table I. The various parameters in Eqs. A1 and A2 were adjusted to give complete inactivation of I_{si} at the end of 300 ms voltage-clamp steps, as indicated by the measurements of Josephson and Sperelakis (1982).

The results of Ebihara and Johnson (1980) and Josephson and Sperelakis (1982) were obtained from aggregates of ventricular cells. We have assumed that their results were appropriate for atrial cells based on the similarity of the upstroke velocities of the action potentials of the two cell types in control and TTX conditions (A. Shrier and J. R. Clay, unpublished).

The models for the I_{x_1} and I_{x_2} kinetics and the I_{x_1} current-voltage relation that we used in these simulations (Table I) were the same as given above. We modeled the I_{x_2} current-voltage relation by the Goldman-Hodgkin-Katz equation (GHK) to be consistent with descriptions of the delayed rectifier in nerve, which appears to be qualitatively similar to I_{x_2} (Frankenhauser, 1962; Binstock and Goldman, 1971; Clay and Shlesinger, 1983). The GHK equation for I_{x_2} is given by (Goldman, 1943; Hodgkin and Katz, 1949)

$$I_{x_2}(s_{x_2} = 1) = PF(eV/kT)$$
$$[K_o - K_i \exp(eV/kT)]/[1 - \exp(eV/kT)], \quad (9)$$

where e is the electronic charge, k is the Boltzmann constant, T is the absolute temperature, F is the Faraday, P is the classically defined permeability coefficient (Table I), and K_o and K_i are the external and internal potassium ion concentrations, respectively.

The background, or time-independent current, I_{bg}, was determined by subtracting the steady-state amplitudes of I_{x_1} and I_{x_2} from the current-voltage relations in Fig. 2. This result was identified with the sum of I_{K_1}, the inward rectifying, background potassium current, and $I_{Na,b}$, the background sodium ion current.

We gratefully acknowledge the technical assistance of R. Brochu who helped carry out some of these experiments, and Dr. R. Siegel for technical assistance in the data analysis.

This work was supported by a grant to A. Shrier from the Medical Research Council, Canada.

Received for publication 4 October 1985 and in final form 12 March 1986.

REFERENCES

Atwell, D., I. Cohen, D. Eisner, M. Ohba, and C. Ojeda. 1979. The steady-state TTX-sensitive ("window") sodium current in cardiac Purkinje fibers. *Pfluegers Arch. Eur. J. Physiol.* 379:137–142.

Beeler, G. W., and H. Reuter. 1977. Reconstruction of the action potential of ventricular myocardial fibers. *J. Physiol. (Lond.).* 268:177–210.

Binstock, L., and L. Goldman. 1971. Rectification in instantaneous potassium current-voltage relations in *Myxicola* giant axons. *J. Physiol.(Lond.).* 217:517–531.

Bristow, D. G., and J. W. Clark. 1982. A mathematical model of primary pacemaking cell in SA node of the heart. *Am. J. Physiol.* 143:H207–H218.

Brown, H. F., A. Clark, and S. J. Noble. 1976. Analysis of pacemaker and repolarization currents in frog atrial muscle. *J. Physiol. (Lond.).* 258:547–577.

Brown, H. F., D. Difrancesco, D. Noble, and S. J. Noble. 1980. The contribution of potassium accumulation to outward currents in frog atrium. *J. Physiol. (Lond.).* 306:127–149.

Brown, H. F., J. Kimura, D. Noble, S. J. Noble, and A. Taudignon. 1984. The ionic currents underlying pacemaker activity in rabbit sino-atrial node: experimental results and computer simulations. *Proc. R. Soc. Lond. B. Biol. Sci.* 222:329–247.

Clay, J. R. 1984. Potassium channel kinetics in squid axons with elevated levels of external potassium concentration. *Biophys. J.* 45:481–485.

Clay, J. R., and R. L. DeHaan. 1979. Fluctuations in interbeat interval in rhythmic heart-cell clusters. Role of membrane voltage noise. *Biophys. J.*28:377–390.

Clay, J. R., and M. F. Shlesinger. 1983. Effects of external cesium and rubidium on outward potassium currents in squid axons. *Biophys. J.* 42:43–53.

Clay, J. R., and M. F. Shlesinger. 1984. Analysis of the effects of cesium ions on potassium channel currents in biological membranes. *J. Theor. Biol.* 107:189–201.

Clay, J. R., and A. Shrier. 1981*a*. Analysis of subthreshold pacemaker currents in chick embryonic heart cells. *J. Physiol. (Lond.).* 312:471–490.

Clay, J. R., and A. Shrier. 1981*b*. Developmental changes in subthreshold pacemaker currents in chick embryonic heart cells. *J. Physiol. (Lond.).* 132:491–504.

Clay, J. R., L. J. DeFelice, and R. L. DeHaan. 1979. Current noise parameters derived from voltage noise and impedance in embryonic heart cell aggregates. *Biophys. J.* 28:169–184.

DeFelice, L. J., and R. L. DeHaan. 1977. Membrane noise and intercellular communication. *Proc. IEEE (Inst. Electr. Electron. Eng.) (Spec. Issue Biol. Signals).* 65:796–799.

DeHaan, R. L. 1967. Regulation of spontaneous activity and growth of embryonic chick heart cells in tissue culture. *Dev. Biol.* 16:216–249.

DeHaan, R. L. 1970. The potassium sensitivity of isolated embryonic heart cells increases with development. *Dev. Biol.* 23:226–240.

DeHaan, R. L., and H. A. Fozzard. 1975. Membrane response to current pulses in spheroidal aggregates of embryonic heart cells. *J. Gen. Physiol.* 65:207–222.

DiFrancesco, D. 1981. A new interpretation of the pace-maker current in calf Purkinje fibers. *J. Physiol.(Lond.).* 314:359–376.

Ebihara, L., and E. A. Johnson. 1980. Fast sodium current in cardiac muscle. *Biophys. J.* 32:779–790.

Ebihara, L., N. Shigeto, M. Lieberman, E. Johnson. 1980. The initial inward current in spherical clusters of chick embryonic heart cells. *J. Gen. Physiol.*75:437–456.

Ebihara, L., N. Shigeto, M. Lieberman, and E. A. Johnson. 1983. A note on the reactivation of the fast sodium current in spherical clusters of embryonic chick heart cells. *Biophys. J.* 42:191–193.

Fischmeister, R., and M. Horackova. 1983. Variation of intracellular Ca^{2+} following Ca^{2+} current in heart. A theoretical study of ionic diffusion inside a cylindrical cell. *Biophys. J.* 41:341–348.

Frankenhauser, B. 1962. Potassium permeability in myelinated nerve fibres of *Xenopus Laevis*. *J. Physiol. (Lond.)* 160:54–61.

Frankenhauser, B., and A. L. Hodgkin. 1956. The after-effects of impulses in the giant nerve fibers of *Loligo*. *J. Physiol. (Lond.).* 131:341–376.

Giles, W. R., and A. C. G. van Ginnekin. 1985. A transient outward current in isolated cells from the crista terminalis of rabbit heart. *J. Physiol.(Lond.).* 368:243–264.

Giles, W. R., and E. F. Shibata. 1985. Voltage clamp of bull-frog cardiac pace-maker cells: A quantitative analysis of potassium currents. *J. Physiol. (Lond.).* 368:265–292.

Gintant, G. A., N. B. Datyner, and I. S. Cohen. 1985. Gating of delayed rectification in acutely isolated canine cardiac Purkinje myocytes. Evidence for a single voltage-gated conductance. *Biophys. J.* 48:1059–1064.

Goldman, D. E. 1943. Potential, impedance, and rectification in membranes. *J. Gen. Physiol.* 27:37–60.

Hodgkin, A. L., and A. F. Huxley. 1952. A quantitative description of membrane current and its application to conduction and excitation in nerve. *J. Physiol.(Lond.).* 117:500–544.

Hodgkin, A. L., and B. Katz. 1949. The effect of sodium ions on the electrical activity of the giant axon of the squid. *J. Physiol. (Lond.).* 108:37–77.

Hume, J. R., and W. Giles. 1983. Ionic current in single isolated bullfrog atrial cells. *J. Gen. Physiol.* 81:153–194.

Jaeger, J. M., and W. R. Gibbons. 1985*a*. A re-examination of late outward plateau currents of cardiac Purkinje fibers. *Am. J. Physiol.* 249:H108–H121.

Jaeger, J. M., and W. R. Gibbons. 1985*b*. Slow inward current may produce many results attributed to I_{x_1} in cardiac Purkinje fibers. *Am. J. Physiol.* 249:H122–H132.

Josephson, I., and N. Sperelakis. 1982. On the ionic mechanism underlying adrenergic-cholinergic antagonism in ventricular muscle. *J. Gen. Physiol.* 79:69–86.

Kass, R. S., and M. C. Sanguinetti. 1984. Calcium channel inactivation in the calf cardiac Purkinje fiber: evidence for voltage- and calcium-mediated mechanisms. *J. Gen. Physiol.* 84:705–726.

Lee, K. S., E. Marban, and R. W. Tsien. 1985. Inactivation of calcium channels in mammalian heart cells: joint dependence on membrane potential and intracellular calcium. *J. Physiol.(Lond.).* 364:395–411.

Mathias, R. T., L. Ebihara, M. Lieberman, E. M. Johnson. 1981. Linear electrical properties of passive and active currents in spherical heart cell clusters. *Biophys. J.* 36:221–242.

McAllister, R. E., D. Noble, and R. W. Tsien. 1975. Reconstruction of the electrical activity of cardiac Purkinje fibres. *J. Physiol. (Lond.).* 251:1–59.

McDonald, T. F., and W. Trautwein. 1978. The potassium current underlying delayed rectification in cat ventricular muscle. *J. Physiol. (Lond.).* 274:217–246.

Moore, J. W., and F. Ramon. 1974. On numerical integration of the Hodgkin and Huxley equations for a membrane action potential. *J. Theor. Biol.* 45:249–273.

Nathan, R. D., and R. L. DeHaan. 1978. In vitro differentiation of a fast Na^+ conductance in embryonic heart cell aggregates. *Proc. Natl. Acad. Sci. USA.* 75:2776–2780.

Nathan, R. D., and R. L. DeHaan. 1979. Voltage-clamp analysis of embryonic heart cell aggregates. *J. Gen. Physiol.* 73:175–198.

Noble, S. 1976. Potassium accumulation and depletion in frog atrial muscle. *J. Physiol. (Lond.).* 258:579–613.

Noble, D. 1984. The surprising heart: a review of recent progress in cardiac electrophysiology. *J. Physiol. (Lond.).* 353:1–50.

Noble, D., and R. W. Tsien. 1968. The kinetics and rectifier properties of the slow potassium current in cardiac Purkinje fibres. *J. Physiol. (Lond.)* 195:185–214.

Noble, D., and R. W. Tsien. 1969. Outward membrane currents activated within the plateau range of potentials in cardiac Purkinje fibres. *J. Physiol. (Lond.).* 200:204–231.

Ojeda, C., and O. Rougier. 1974. Kinetic analysis of the delayed outward currents in frog atrium. Existence of two types of preparation. *J. Physiol. (Lond.).* 239:51–73.

Rissanen, J. 1978. Modeling by shortest data description. *Automatica.* 14:465–471.

Rush, S., and H. Larsen. 1978. A practical algorithm for solving dynamic membrane equations. *IEEE (Inst. Electr. Electron. Eng.) Trans. Biomed. Eng.* 25:389–392.

Sachs, H., and R. L. DeHaan. 1973. Embryonic myocardial cell aggregates: volume and pulsation rate. *Dev. Biol.* 30:223–240.

Shrier, A., and J. R. Clay. 1980. Pacemaker currents in chick embryonic heart cells change with development. *Nature (Lond.).* 283:670–671.

Shrier, A., and J. R. Clay. 1982. Comparison of the pacemaker properties of chick embryonic atrial and ventricular heart cells. *J. Membr. Biol.* 69:49–56.

Shrier, A., J. R. Clay, and R. M. Brochu. 1984. Analysis of repolarization currents in chick embryonic heart cell aggregates. *Biophys. J.* 45(2, Pt. 2):55*a*. (Abstr.)

Yanagihara, K., A. Noma, and H. Irisawa. 1980. Reconstruction of sinoatrial node pacemaker potential based on the voltage clamp experiments. *Jpn. J. Physiol.* 30:841–857.